Research Square

Preprints are preliminary reports that have not undergone peer review.
They should not be considered conclusive, used to inform clinical practice,
or referenced by the media as validated information.

Residual ovarian androgens induce local estrogen synthesis as a compensatory mechanism that regulates inflammatory pain in peripheral sensory neurons

Hyeryeong Lee
Chungnam National University
Sheu-Ran Choi
Catholic Kwandong University College of Medicine
Hyunjin Shin
Chungnam National University
Jaehong Park
Chungnam National University
Miae Lee
Chungnam National University
Miok Bae
Daegu Health College
Yeonhee Ryu
Korea Institute of Oriental Medicine
Suk-Yun Kang
Korea Institute of Oriental Medicine
Chang Woo Chae
Chungnam National University
Hyun-Woo Kim
kim0827@cnu.ac.kr

Chungnam National University

Article

Keywords:

Posted Date: November 18th, 2026

DOI: https://doi.org/10.21203/rs.3.rs-11424145/v1

License: This work is licensed under a Creative Commons Attribution 4.0 International License.
Read Full License

Additional Declarations: No competing interests reported.

Residual ovarian androgens induce local estrogen synthesis as a compensatory mechanism that regulates inflammatory pain in peripheral sensory neurons

Hyeryeong Lee [a]† , Sheu-Ran Choi[b]†, Hyunjin Shin[a], Jaehong Park[a], Miae Lee[a], Miok Bae[c], Yeonhee Ryu[d], Suk-Yun Kang[d], Chang Woo Chae[a], Hyun-Woo Kim[a*]

[a]Department of Physiology and Medical Science, College of Medicine and Brain Research Institute, Chungnam National University, Daejeon, Republic of Korea

[b]Department of Pharmacology, Catholic Kwandong University College of Medicine, Gangneun, Republic of Korea

[c]D.V.M., M.S. Preclinical Research Center, Department of Pet Health Management, Daegu Health College, Daegu, 41453, Republic of Korea

[d]KM Fundamental Research Division, Korea Institute of Oriental Medicine, Daejeon, Republic of Korea

†These authors contribute equally to this study

Hyun-Woo Kim

Department of Physiology and Medical Science, College of Medicine and Brain Research Institute, Chungnam National University, Daejeon 35015, Republic of Korea. E-mail: kim0827@cnu.ac.kr, Tel: +82-42-580-8217, Fax: +82-42-585-8440

1. Introduction

Hormones are well known to play important roles in maintaining structural and functional homeostasis in both the nervous system and peripheral target organs.[1,2] In particular, in women, estrogen is primarily synthesized in the ovaries and exerts widespread effects on the central and peripheral nervous systems via estrogen receptor-dependent signaling following systemic circulation.[3] Furthermore, estrogen can regulate tissue-specific neural function through local synthesis mediated by aromatase.[4]

As women age, menopause occurs as a consequence of ovarian follicle depletion, resulting in a progressive decline in female hormone levels.[5] This transition should not be viewed simply as a decrease in female hormones, but rather as a process of systemic reprogramming driven by the loss of ovarian function.[6] During the reproductive period, hormonal fluctuations associated with the menstrual cycle continuously shape physiological function. Accordingly, the body adapts to these changes through plastic modifications of its systems, including the nervous system.[7]

Previous studies have demonstrated that estrogen depletion enhances nociceptive responses within the sensory nervous system involved in pain processing and increases neuronal excitability in the spinal cord.[8,9] Although ovariectomy models have been extensively used to investigate the effects of hormone depletion, they are limited by the rapid decline in circulating estrogen levels following ovarian removal and their inability to reproduce androgen production by residual ovarian tissue after follicular depletion.[10,11]

The VCD model addresses these limitations by selectively accelerating the depletion of primordial and primary follicles through repeated administration while preserving residual ovarian tissue capable of producing estrogen precursors.[12,13] Unlike the ovariectomy (OVX) model, which involves complete removal of the ovaries, the VCD model can more accurately reflect the adaptive changes in the sensory nervous system that occur during the gradual decline in hormone levels associated with ovarian dysfunction.[14] However, little is known about how the preservation of residual ovarian tissue influences

structural and functional adaptations within the sensory nervous system. Therefore, further studies are required to clarify the adaptive neural changes and underlying mechanisms associated with residual ovarian function.

We investigated whether androstenedione secreted from residual ovarian tissue influences neural adaptations induced by estrogen depletion in the peripheral nervous system by comparing the conventional estrogen-deficient OVX model with a follicular depletion-induced VCD model. In the conventional VCD model, estrous arrest resulting from follicular depletion typically occurs 90–100 days after the completion of a 20-day administration regimen. Consequently, the prolonged administration period and delayed onset of follicular depletion can reduce experimental efficiency. To overcome these limitations, we developed a novel administration protocol. This modified model improved experimental efficiency by shortening the time required to induce follicular depletion while preserving the physiological advantages of the VCD model. Furthermore, by maintaining the functional integrity of residual ovarian tissue, the model enabled a more effective evaluation of adaptive changes in the peripheral sensory nervous system and pain regulatory mechanisms under menopause-like conditions.

2. Results

2.2 Physiological changes induced by different hormone depletion models

We compared body weight gain, ovarian morphology, uterine parameters, and circulating hormone concentrations among three hormone depletion models established using different approaches. Female mice subjected to OVX exhibited a significantly greater increase in body weight compared with control mice. In addition, body weight was significantly increased from 10 days post-surgery in the OVX group compared with the IP-VCD and IO-VCD groups, in which ovarian failure was induced while preserving ovarian tissue (Figs. 2b and c). To evaluate the effects of hormone depletion on reproductive organs, uterine weight and diameter were assessed. Marked uterine atrophy was observed in the OVX group. Although uterine weight and diameter were significantly reduced in both the IP-VCD and IO-VCD groups compared with the control group, these parameters remained significantly greater than those in the OVX group (Figs. 2d–g). Analysis of circulating hormone levels revealed that serum estradiol concentrations were significantly decreased in the OVX, IP-VCD, and IO-VCD groups compared with the control groups. In contrast, serum androstenedione concentrations were significantly higher in the IP-VCD and IO-VCD groups than in the OVX group (Figs. 2h and i). These findings suggest that residual ovarian tissue in the ovarian failure models retains the capacity to produce androstenedione. Furthermore, they indicate that preservation of ovarian tissue is a key determinant of differences in the endogenous hormonal environment following hormone depletion.

2.3 VCD selectively depletes follicles.

VCD selectively induces apoptosis in primordial follicles, resulting in follicular depletion[14]. To compare follicular depletion induced by intraperitoneal and intraovarian administration of VCD and to determine whether the IO-VCD model reproduced the follicular depletion observed in the conventional IP-VCD model, ovarian tissues were subjected to histological analysis following H&E staining (Fig. 3a). In both

the IP-VCD and IO-VCD groups, the numbers of primary, secondary, and antral follicles were significantly reduced compared with those in the control group at the time corresponding to persistent estrous arrest (Figs. 3b–d). These findings demonstrate that intraovarian administration of VCD induces selective follicular depletion comparable to that produced by conventional intraperitoneal administration.

2.4 Female hormone depletion increased depression-like behaviors without differences among hormone depletion models

Female hormones are known to influence emotional regulation in women.[15,16] Therefore, we investigated the effects of hormone depletion on emotional behaviors (Fig. 4a). In the open field test, no significant differences were observed among the groups in total distance traveled, time spent in the center zone, or the number of center zone entries (Figs. 4b–e). In the forced swim test, all three hormone depletion models exhibited significantly increased immobility time compared with the control group; however, no significant differences were observed among the OVX, IP-VCD, and IO-VCD groups (Fig. 4f). These results indicate that hormone depletion did not affect exploratory behavior or locomotor activity but significantly increased depression-like behavior. Moreover, differences in the methods used to induce hormone depletion did not influence exploratory behavior, locomotor activity, or depression-like behavior.

2.5 Effects of Residual Ovarian Tissue Following Follicular Depletion on Formalin-Induced Inflammatory Pain

To determine whether preservation of ovarian tissue following follicular depletion influences inflammatory pain responses, formalin was injected into the plantar surface of the right hind paw. Male

mice were included to assess whether the effects of hormone depletion were sex-dependent. Pain behaviors were analyzed during the first and second phases of the formalin test (Fig. 5a). No significant differences in pain behavior were observed among the hormone depletion models during the first phase (Fig. 5b). In contrast, during the second phase, the OVX group exhibited significantly greater pain behavior than the sham group (Fig. 5c). Conversely, the male, IP-VCD, and IO-VCD groups showed significantly reduced pain behavior compared with the OVX group.

To determine whether these behavioral differences were associated with neuronal activation in the spinal cord, c-Fos immunohistochemistry was performed in the dorsal horn following formalin administration (Fig. 5d). Quantitative analysis of c-Fos-positive neurons in laminae I–II of the dorsal horn revealed a significant increase in the OVX group compared with the sham, male, IP-VCD, and IO-VCD groups. No significant differences were observed among the sham, male, IP-VCD, and IO-VCD groups (Fig. 5e). These findings indicate that preservation of ovarian tissue attenuates formalin-induced second-phase pain behavior and spinal neuronal activation following follicular depletion.

2.6 Changes in DRG Aromatase Expression Following Hormone Depletion

To investigate the mechanism underlying the differences in spinal neuronal activity observed among the hormone depletion models during formalin-induced pain, the expression of aromatase, an estrogen-synthesizing enzyme, was examined in the DRG. Immunofluorescence analysis revealed that aromatase did not colocalize with glutamine synthetase (GS), a marker of satellite glial cells, but colocalized with NeuN, a neuronal marker (Figs. 6a and b). These findings indicate that aromatase is primarily expressed in DRG sensory neurons. Analysis of aromatase expression according to neuronal size demonstrated that aromatase expression was highest in small-diameter neurons (< 25 μm) compared with medium-diameter (25–35 μm) and large-diameter (> 35 μm) neurons (Fig. 6c–f). Although aromatase was expressed in the DRG of male mice, its expression level did not differ significantly from that of the intact female group. In contrast, the IP-VCD and IO-VCD groups exhibited significantly higher

aromatase expression in both small- and medium-diameter neurons than the intact, male, and OVX groups. These findings suggest that increased aromatase expression in small- and medium-diameter neurons of DRG may contribute to the regulation of peripheral inflammatory pain.

2.7 Effects of Aromatase Inhibition on Peripheral Inflammatory Pain in Follicle-Decreasing Estrogen-Decreasing Models

As aromatase expression was significantly increased in the DRG of the IP-VCD and IO-VCD model, we investigated whether inhibition of aromatase affects formalin-induced inflammatory pain. Mice received a single intraperitoneal administration of letrozole, a standard aromatase inhibitor, before the formalin test (Fig. 7a). No significant differences in licking behavior were observed between the letrozole-treated and Existing IP-VOD or IO-VCD groups during the first phase (Fig. 7b). Second phase pain behaviors in IP-VCD and IO-VCD groups administered with Letrozole increased compared to standard IP-VCD and IO-VCD models (Fig. 7c). In addition, the reduction in formalin-induced spinal neuronal activation observed in the IP-VCD and IO-VCD models was reversed by administration of letrozole, as indicated by increased c-Fos expression in the spinal dorsal horn (Figs 7d and e). These findings suggest that activation of aromatase contributes to the attenuation of formalin-induced inflammatory pain in the follicular depletion models.

3. Discussion

In this study, we demonstrated that the method used to induce hormone depletion differentially affects endocrine function and sensory nervous system adaptations by comparing the OVX, conventional IP-VCD, and a newly established IO-VCD models. VCD induces follicular depletion by triggering apoptosis of ovarian follicles through disruption of the PI3K/Akt signaling pathway, resulting in the selective loss of primordial and primary follicles.[18,19,20,21] To improve the efficiency of the conventional VCD model, we established an intraovarian VCD administration protocol that allows direct delivery of VCD to the ovary. Compared with the conventional IP-VCD model, the IO-VCD model accelerated persistent estrous cycle arrest by approximately 50 days while producing a comparable degree of follicular depletion. Histological analysis performed after persistent estrous cycle arrest demonstrated a significant reduction in follicle number in both the IP-VCD and IO-VCD models compared with the control group. These findings suggest that intraovarian administration enhances follicular toxicity by directly exposing early-stage follicles to VCD. In the conventional IP-VCD model, VCD must first enter the systemic circulation before reaching the ovaries, requiring relatively high cumulative doses to induce follicular depletion.[22] In contrast, intraovarian administration maintains a high local concentration of VCD within the ovarian microenvironment while using a substantially lower dose. Consequently, the IO-VCD model provides a rapid and physiologically relevant model of follicular depletion that preserves residual ovarian tissue and facilitates the investigation of menopause-associated endocrine and sensory adaptations.

Regarding overall physiological changes, the OVX model exhibited the greatest body weight gain, whereas neither the IP-VCD nor the IO-VCD model showed significant changes in body weight compared with the control group compared with the control group. Although the effects of estrogen and androgens on body weight regulation and adiposity are influenced by multiple metabolic factors[23,24], this difference may be attributed to the preservation of residual ovarian tissue in the IP-VCD and IO-VCD models, which likely retains the capacity to produce androstenedione and other steroid hormones.

Previous studies have shown that VCD selectively depletes ovarian follicles while preserving the steroidogenic function of ovarian stromal cells.[25] Consistent with these observations, the serum hormone analyses in the present study demonstrated that residual endocrine function was preserved in both the IP-VCD and IO-VCD models.

Estrogen plays a critical role in the growth and maintenance of uterine tissue through activation of uterine estrogen receptor α (ERα) and estrogen receptor β (ERβ), and estrogen deficiency is well known to induce uterine atrophy.[25,26] Consistent with these observations, the present study demonstrated marked uterine atrophy and a significant reduction in uterine weight in the OVX model, confirming the physiological consequences of abrupt estrogen depletion. In contrast, uterine weight and morphology were relatively preserved in the IP-VCD and IO-VCD models compared with the OVX model. Previous studies have shown that androstenedione administration increases uterine weight in OVX animals [27] Therefore, residual ovarian androstenedione may have contributed to the preservation of uterine structure in the IP-VCD and IO-VCD models. In addition, circulating androstenedione may have been locally converted to estrogen by aromatase in peripheral tissues, including the uterus, thereby contributing to the maintenance of uterine morphology.[28,29]

In the present study, we investigated the effects of hormone depletion on the peripheral sensory nervous system using three hormone depletion models. Male mice did not exhibit significant differences in formalin-induced pain behavior compared with intact female mice, consistent with previous studies demonstrating that testosterone contributes to pain regulation in males.[30] Formalin-induced inflammatory pain behavior was significantly attenuated in the IP-VCD and IO-VCD models compared with the OVX model. Consistent with these behavioral findings, neuronal activation in the spinal dorsal horn was significantly greater in the OVX model than in the IP-VCD and IO-VCD models. Collectively, these findings suggest that hyperalgesia associated with estrogen depletion may be attenuated by residual ovarian steroidogenic activity. Estrogen receptors are widely expressed throughout nociceptive pathways, where estrogen modulates pain signaling through estrogen receptor-dependent mechanisms [31,14] Previous studies have demonstrated that locally synthesized estrogen within the spinal dorsal horn

contributes to pain modulation.[32,14] In addition, estrogen produced within the DRG has been proposed to regulate nociceptive signaling through interactions with calcium channels, ion channels, and TRPV1 following activation of estrogen receptors.[33,34]

Aromatase is the key enzyme responsible for local estrogen synthesis by converting androstenedione into estrogens.[35] In the present study, aromatase expression was detected in DRG sensory neurons in all experimental groups, suggesting that locally synthesized estrogens may participate in the regulation of nociceptive signaling at the level of primary sensory neurons. Notably, aromatase expression was significantly increased in the IP-VCD and IO-VCD models, whereas no significant differences were observed among the OVX, male, and intact female groups. Previous studies have demonstrated that circulating estrogens directly regulate sensory neuronal function in females, whereas androgens contribute to pain modulation in males through distinct mechanisms.[36] Therefore, the selective upregulation of aromatase in the IP-VCD and IO-VCD models may represent a unique adaptive response associated with the preservation of residual ovarian function following follicular depletion.

Unlike the OVX model, which lacks residual ovarian steroidogenic activity, the IP-VCD and IO-VCD models preserve ovarian tissue capable of producing steroid hormone precursors, including androstenedione. Therefore, systemic estrogen deficiency combined with preserved residual ovarian function may induce a compensatory increase in aromatase expression, potentially facilitating local estrogen production within DRG sensory neurons and contributing to pain regulation. Notably, aromatase expression in the IP-VCD and IO-VCD models was most prominent in small-diameter sensory neurons. These neurons predominantly consist of nociceptive C-fibers and Aδ-fibers that transmit mechanical, thermal, and inflammatory nociceptive stimuli.[37] Therefore, increased aromatase expression in these neurons may contribute to the modulation of nociceptive signaling. This interpretation is supported by the finding that administration of letrozole, an aromatase inhibitor, reversed the attenuation of formalin-induced pain behavior and restored spinal neuronal activation in the IP-VCD and IO-VCD models.

In conclusion, residual ovarian function preserved in follicular depletion models, rather than

ovariectomy, may partially compensate for systemic estrogen deficiency through the maintenance of residual steroidogenic activity. Notably, the increased expression of aromatase in peripheral sensory neurons suggests that aromatase-dependent mechanisms contribute to the regulation of inflammatory pain under estrogen-deficient conditions, potentially through local estrogen production. Furthermore, the IP-VCD and IO-VCD models more closely mimic the gradual decline in ovarian function associated with natural menopause and may therefore provide physiologically relevant models for investigating adaptive changes in the peripheral sensory nervous system. Aromatase inhibitors such as letrozole are widely used in the treatment of hormone receptor-positive breast cancer in postmenopausal women.[38] Given the potential role of aromatase in sensory neuronal adaptation, the present findings raise the possibility that long-term aromatase inhibition may influence sensory nervous system function under postmenopausal conditions.

4. Methods

4.1 Mice

All animal experiments were approved by the Animal Ethics Committee of Chungnam National University College of Medicine, Korea, and were conducted in accordance with its guidelines. ICR female mice (7–8 weeks old) and ICR male mice (7–8 weeks old) were purchased from Samtako Bio (Samtako Bio Inc, Korea). The animals were housed in a facility with a temperature (22±2°C) and humidity (30–60%) maintaining a 12-hour day-dark cycle, and water and food intake were unrestricted. All mice were acclimatized in the animal facility for one week prior to the experiments.

Mice designated for euthanasia were humanely killed by allowing them to inhale CO_2 within a chamber connected to a CO_2 supply system. The chamber containing the mice was gradually filled with the gas at a flow rate equivalent to 10%–30% of the chamber's volume per minute. Once cardiac arrest was confirmed, the gas supply was discontinued. Mice selected for tissue collection for immunohistochemical analysis were anesthetized via an intraperitoneal injection of Avertin (12.5 mg/mL; 215.5 mg/kg, i.p injection). Subsequently, transcardial perfusion was performed using a perfusion pump to sequentially deliver phosphate-buffered saline (PBS) and 4% paraformaldehyde (PFA).

4.2 Hormone depletion induction model

Three hormone depletion models were established: the OVX model, the intraperitoneal injection of VCD (IP-VCD) model, and the intraovarian injection of VCD (IO-VCD) model (Fig. 1). For the OVX model, animals were deeply anesthetized with Avertin prior to surgery. Small bilateral flank incisions were made, and the ovarian fat pads were carefully exteriorized using surgical forceps. The uterine horns were ligated with surgical sutures to prevent bleeding, and both ovaries were subsequently removed. The incision sites were sutured and disinfected, and the animals were allowed to recover under

standard postoperative conditions. Sham-operated animals underwent the same surgical procedure, except that the ovaries were left intact. For the IP-VCD model, 4-vinylcyclohexene diepoxide (160 mg/kg; Sigma-Aldrich, St. Louis, MO, USA) was administered intraperitoneally once daily for 20 consecutive days using corn oil (Sigma-Aldrich, St. Louis, MO, USA) as the vehicle. Vehicle-treated mice received an equivalent volume of corn oil alone. For the IO-VCD model, animals were anesthetized with Avertin prior to surgery. Bilateral flank incisions were made, and the ovarian fat pads were gently exteriorized using forceps. A 5 μL volume of VCD solution was injected using a Hamilton syringe fitted with a 30-gauge needle. The needle was carefully advanced through the ovarian fat pad into the ovarian bursa surrounding the ovary. To minimize tissue damage, the needle was maintained at a fixed angle with minimal movement during the injection. Following administration of the VCD solution, the needle was left in place for 20 s to prevent leakage. In all three models, hormone depletion was defined as the absence of estrous cycle for more than 5 consecutive days.

[Figure 1.]

4.3 Mouse estrus cycle analysis

To assess hormone depletion, vaginal cytology was performed as a primary screening method. A sterile micro-swab moistened with saline was gently inserted into the vagina of each mouse and rotated once along the vaginal wall before being withdrawn. Vaginal cells collected on the swab were evenly transferred onto a glass slide by rolling the swab across the slide surface. After air-drying, the slides were immersed in crystal violet solution for 1 minute and subsequently rinsed in triple-distilled water for 1 minute. The washing step was repeated twice. Following staining, 15 μL of glycerol was applied to the stained area, and the slide was covered with a coverslip.

4.4 Serum hormone measurement

Blood was collected by cardiac puncture from deeply anesthetized mice and allowed to clot at room temperature (23–26°C) for 1 h. Samples were then centrifuged at 5,000 rpm for 15 minutes at 4°C, and the resulting serum was collected for analysis. Serum estradiol and androstenedione concentrations were quantified according to the manufacturers' instructions using a high-sensitivity competitive estradiol ELISA kit (Enzo Life Sciences, Farmingdale, NY, USA) and an androstenedione ELISA kit (Arbor Assays, Ann Arbor, MI, USA), respectively. Absorbance was measured at 405 nm and 450 nm using a microplate reader, and all samples were analyzed in duplicate. Hormone concentrations were calculated using a four-parameter logistic (4PL) regression model.

4.5 Histological analysis

Ovarian and uterine tissues were fixed in 4% paraformaldehyde (PFA) for 24 h, embedded in paraffin, and sectioned using a microtome (Leica Microsystems, Wetzlar, Germany). Uterine tissues were serially sectioned at a thickness of 8 μm, whereas ovarian tissues were sectioned at 5 μm and subsequently stained with hematoxylin and eosin (H&E). Uterine diameter was measured using ImageJ software. For ovarian analysis, every 20th section throughout the entire ovary was collected for histological evaluation. Follicles were classified as primary, secondary, or antral follicles based on their morphological characteristics. Primary follicles were identified by a single layer of cuboidal granulosa cells surrounding the oocyte. Secondary follicles contained two or more layers of granulosa cells, whereas antral follicles were characterized by the presence of a distinct antral cavity[33]. The total number of follicles per ovary was calculated by summing the follicle counts from all analyzed sections.

4.6 Open field test

The open field test was performed to evaluate exploratory behavior and locomotor activity in the hormone depletion mouse models. Mice were placed in the center of a black open-field arena (40 × 40 cm) and allowed to explore freely for 5 min following a 30-s habituation period. Total distance traveled

(cm), time spent in the center zone, and the number of entries into the center zone were recorded. Animal behavior was monitored using a video camera positioned above the arena. Locomotor activity and behavioral parameters were analyzed using EthoVision XT 11.5 software (Noldus Information Technology, Wageningen, The Netherlands).

4.7 Forced swim test

The forced swimming test (FST) was performed according to a previously published protocol.[40] A Plexiglas cylinder (10 × 25 cm) was filled with water maintained at 24 ± 0.5 °C to a depth of 15 cm. Animals were placed individually into the cylinder and allowed a 1-minute habituation period, followed by a 5-minute test session. The initial 1 min was considered an adaptation period during which immediate escape-oriented behaviors were observed. Subsequently, immobility was recorded for 5 minutes. Immobility was defined as the absence of active movements, with the animal remaining afloat and making only the minimal movements necessary to keep its head above the water surface. Active behavior was defined as swimming, climbing, or vigorous struggling movements.

4.8 Formalin test

The formalin test was performed to assess nociceptive behavior. Mice were individually placed in a transparent acrylic chamber (40 cm in height and 20 cm in diameter) and allowed to habituate to the testing environment for 30 minutes. Following habituation, 20 μL of 5% formalin was injected subcutaneously into the plantar surface of the right hind paw using a 30-gauge needle. Pain-related behaviors were recorded using a video camera for a total of 60 minutes. Licking or biting of the formalin-injected paw was considered nociceptive behavior, and the cumulative duration of these behaviors was quantified in 5-min intervals. Behavioral responses were analyzed in two phases: 1st Phase (0–15 minutes), representing the acute nociceptive response, and 2nd Phase (15–60 minutes), representing the inflammatory and central sensitization-related response.

4.9 Immunohistochemistry

Three hours after formalin injection, mice were deeply anesthetized with Avertin and transcardially perfused with cold phosphate-buffered saline (PBS), followed by 4% PFA. The vertebral columns containing the spinal cord and dorsal root ganglia (DRG) were dissected and post-fixed in 4% PFA at 4°C for 24 h. The tissues were then cryoprotected in 30% sucrose until they sank. The L4–L6 spinal cord segments and corresponding DRG were sectioned using a cryostat (Leica Microsystems, Wetzlar, Germany). Spinal cord tissues were sectioned at 25 μm, whereas DRG tissues were sectioned at 10 μm. DRG sections were mounted onto coated glass slides, while free-floating spinal cord sections were collected in PBS.

For immunohistochemical staining, DRG sections were permeabilized with PBS containing 0.1% Triton X-100 for 30 min and blocked with 3% bovine serum albumin (BSA) for 1 h at room temperature. Spinal cord sections were permeabilized with PBS containing 0.01% Triton X-100 for 30 min and blocked with 5x General-Block solution (TransLab, Daejeon, Korea) for 1 h at room temperature. The sections were then incubated overnight at 4°C with the following primary antibodies: anti-aromatase (1:500, cat# 16554-1-AP; Proteintech, Rosemont, IL, USA), anti-glutamine synthetase (GS, 1:500, cat# 610517; BD Biosciences, San Jose, CA, USA), anti-NeuN (1:500, cat# ab104224; Abcam, Cambridge, UK), and anti-c-Fos (1:1,000, cat# ab209794; Abcam, Cambridge, UK). After washing with PBS, the sections were incubated with the appropriate Cy3-conjugated (1:2,000; Jackson ImmunoResearch, West Grove, PA, USA) or FITC-conjugated (1:1,000; Jackson ImmunoResearch, West Grove, PA, USA) secondary antibodies for 60 min at room temperature. The sections were mounted with a DAPI-containing mounting medium (Vector Laboratories, Newark, CA, USA) and coverslipped. Fluorescence images were acquired using a fluorescence microscope (Axio Scope A1; Carl Zeiss, Oberkochen, Germany) and analyzed using ImageJ software (National Institutes of Health, Bethesda, MD, USA).

4.10 Drug administration

Letrozole (Sigma-Aldrich, St. Louis, MO, USA) was dissolved in Dimethyl sulfoxide (DMSO) and diluted with sterile saline to a final concentration of 0.2 mg/mL containing 2% DMSO. Mice received a single intraperitoneal injection of letrozole (1 mg/kg) 45 minutes before the formalin test.

2.11 Statistical analysis

All data are presented as mean ± standard error of the mean (SEM). Comparisons between two groups were performed using an unpaired two-tailed Student's t-test. For comparisons involving three or more groups, one-way analysis of variance (ANOVA) followed by Bonferroni post hoc test was used. A p-value of less than 0.05 was considered statistically significant. Graphs and statistical analyses were performed using GraphPad Prism software (GraphPad Software, San Diego, CA, USA).

References

[1] Jett, S. et al. Ovarian steroid hormones: A long overlooked but critical contributor to brain aging and Alzheimer's disease. Front. Aging Neurosci. 14, 948219; doi:10.3389/fnagi.2022.948219 (2022).

[2] McEwen, B. S. Invited review: Estrogens effects on the brain: Multiple sites and molecular mechanisms. J. Appl. Physiol. 91, 2785–2801; doi:10.1152/jappl.2001.91.6.2785 (2001).

[3] McEwen, B. S. The molecular and neuroanatomical basis for estrogen effects in the central nervous system. J. Clin. Endocrinol. Metab. 84, 1790–1797; doi:10.1210/jcem.84.6.5761 (1999).

[5] Baker, T. G. A quantitative and cytological study of germ cells in human ovaries. Proc. R. Soc. Lond. B Biol. Sci. 158, 417–433; doi:10.1098/rspb.1963.0055 (1963).

[6] Liu, X., Zhao, Y., Feng, Y., Wang, S. & Zhang, J. Ovarian aging: Mechanisms, age-related disorders, and therapeutic interventions. MedComm 6, e70481; doi:10.1002/mco2.70481 (2025).

[7] Gutierrez-Castellanos, N., Husain, B. F. A., Dias, I. C. & Lima, S. Q. Neural and behavioral plasticity across the female reproductive cycle. Trends Endocrinol. Metab. 33, 769–785; doi:10.1016/j.tem.2022.09.001 (2022).

[8] Hassan, S., Muere, A. & Einstein, G. Ovarian hormones and chronic pain: A comprehensive review. Pain 155, 2448–2460; doi:10.1016/j.pain.2014.08.027 (2014).

[9] Li, L.-H., Wang, Z.-C., Yu, J. & Zhang, Y.-Q. Ovariectomy results in variable changes in nociception, mood and depression in adult female rats. PLoS ONE 9, e94312; doi:10.1371/journal.pone.0094312 (2014).

[10] Fogle, R. H., Stanczyk, F. Z., Zhang, X. & Paulson, R. J. Ovarian androgen production in postmenopausal women. J. Clin. Endocrinol. Metab. 92, 3040–3043; doi:10.1210/jc.2007-0581 (2007).

[11] Sluijmer, A. V., Heineman, M. J., Jong, F. H. D. & Evers, J. L. Endocrine activity of the postmenopausal ovary: The effects of pituitary down-regulation and oophorectomy. J. Clin. Endocrinol. Metab. 80, 2163–2167; doi:10.1210/jcem.80.7.7608272 (1995).

[12] Magoffin, D. A. Ovarian theca cell. Int. J. Biochem. Cell Biol. 37, 1344–1349; doi:10.1016/j.biocel.2005.01.016 (2005).

[13] Rivera, Z., Christian, P. J., Marion, S. L., Brooks, H. L. & Hoyer, P. B. Steroidogenic capacity of residual ovarian tissue in 4-vinylcyclohexene diepoxide-treated mice. Biol. Reprod. 80, 328–336; doi:10.1095/biolreprod.108.070359 (2009).

[14] Brooks, H. L., Pollow, D. P. & Hoyer, P. B. The VCD mouse model of menopause and perimenopause for the study of sex differences in cardiovascular disease and the metabolic syndrome. Physiology 31, 250–257; doi:10.1152/physiol.00057.2014 (2016).

[14] Tran, M., Kuhn, J. A., Bráz, J. M. & Basbaum, A. I. Neuronal aromatase expression in pain processing regions of the medullary and spinal cord dorsal horn. J. Comp. Neurol. 525, 3414–3428; doi:10.1002/cne.24269 (2017).

[15] Freeman, E. W. et al. Hormones and menopausal status as predictors of depression in women in transition to menopause. Arch. Gen. Psychiatry 61, 62–70; doi:10.1001/archpsyc.61.1.62 (2004).

[16] Jacobs, E. G. et al. 17β-Estradiol differentially regulates stress circuitry activity in healthy and depressed women. Neuropsychopharmacology 40, 566–576; doi:10.1038/npp.2014.203 (2015).

[17] Todd, A. J. Neuronal circuitry for pain processing in the dorsal horn. Nat. Rev. Neurosci. 11, 823–836; doi:10.1038/nrn2947 (2010).

[18] Fernandez, S. M. et al. Involvement of the KIT/KITL signaling pathway in 4-vinylcyclohexene diepoxide-induced ovarian follicle loss in rats. Biol. Reprod. 79, 318–327; doi:10.1095/biolreprod.108.067744 (2008).

[19] Hu, X., Christian, P., Sipes, I. G. & Hoyer, P. B. Expression and redistribution of cellular Bad, Bax, and Bcl-xL protein is associated with VCD-induced ovotoxicity in rats. Biol. Reprod. 65, 1489–1495; doi:10.1095/biolreprod65.5.1489 (2001).

[20] Kao, S.-W., Sipes, I. G. & Hoyer, P. B. Early effects of ovotoxicity induced by 4-vinylcyclohexene diepoxide in rats and mice. Reprod. Toxicol. 13, 67–75; doi:10.1016/S0890-6238(98)00061-6 (1999).

[21] Springer, L. N. et al. Involvement of apoptosis in 4-vinylcyclohexene diepoxide-induced ovotoxicity in rats. Toxicol. Appl. Pharmacol. 139, 394–401; doi:10.1006/taap.1996.0180 (1996).

[22] Bajaj, G. & Yeo, Y. Drug delivery systems for intraperitoneal therapy. Pharm. Res. 27, 735–738; doi:10.1007/s11095-009-0031-z (2010).

[23] Brown, L. M., Gent, L., Davis, K. & Clegg, D. J. Metabolic impact of sex hormones on obesity. Brain Res. 1350, 77–85; doi:10.1016/j.brainres.2010.04.056 (2010).

[25] Critchley, H. O. D. & Saunders, P. T. K. Hormone receptor dynamics in a receptive human endometrium. Reprod. Sci. 16, 191–199; doi:10.1177/1933719108331121 (2009).

[25] Moccia, P., Belda-Montesinos, R., Monllor-Tormos, A., Chedraui, P. & Cano, A. Body weight and fat mass across the menopausal transition: Hormonal modulators. Gynecol. Endocrinol. 38, 99–104; doi:10.1080/09513590.2021.2004395 (2022).

[26] Mödder, U. I. L. et al. Dose-response of estrogen on bone versus the uterus in ovariectomized mice. Eur. J. Endocrinol. 151, 503–510; doi:10.1530/eje.0.1510503 (2004).

[28] Barakat, R., Oakley, O., Kim, H., Jin, J. & Ko, C. J. Extra-gonadal sites of estrogen biosynthesis and function. BMB Rep. 49, 488–496; doi:10.5483/BMBRep.2016.49.9.141 (2016).

[28] Mennenga, S. E. et al. Pharmacological blockade of the aromatase enzyme, but not the androgen receptor, reverses androstenedione-induced cognitive impairments in young surgically menopausal rats. Steroids 99, 16–25; doi:10.1016/j.steroids.2014.08.010 (2015).

[29] Bulun, S. E., Zeitoun, K., Sasano, H. & Simpson, E. R. Aromatase in aging women. Semin. Reprod. Endocrinol. 17, 349–358; doi:10.1055/s-2007-1016244 (1999).

[30] Craft, R. M., Mogil, J. S. & Aloisi, A. M. Sex differences in pain and analgesia: The role of gonadal hormones. Eur. J. Pain 8, 397–411; doi:10.1016/j.ejpain.2004.01.003 (2004).

[31] Rodríguez-Palma, E. J. et al. Estradiol modulates the role of the spinal α6-subunit containing GABAA receptors in female rats with neuropathic pain. Eur. J. Pharmacol. 974, 176616; doi:10.1016/j.ejphar.2024.176616 (2024).

[32] Chaban, V. Estrogen and visceral nociception at the level of primary sensory neurons. Pain Res. Treat. 2012, 960780; doi:10.1155/2012/960780 (2012).

[33] Chaban, V. Estrogen modulation of visceral nociceptors. Curr. Trends Neurol. 7, 51–55 (2013).

[34] Xu, S., Cheng, Y., Keast, J. R. & Osborne, P. B. 17β-Estradiol activates estrogen receptor β-signalling and inhibits transient receptor potential vanilloid receptor 1 activation by capsaicin in adult rat nociceptor neurons. Endocrinology 149, 5540–5548; doi:10.1210/en.2008-0278 (2008).

[35] Eissa, M. A. & Gohar, E. Y. Aromatase enzyme: Paving the way for exploring aromatization for cardio-renal protection. Biomed. Pharmacother. 168, 115832; doi:10.1016/j.biopha.2023.115832 (2023).

[36] Mogil, J. S. Qualitative sex differences in pain processing: Emerging evidence of a biased literature. Nat. Rev. Neurosci. 21, 353–365; doi:10.1038/s41583-020-0310-6 (2020).

[37] Jang, K. & Garraway, S. M. A review of dorsal root ganglia and primary sensory neuron plasticity mediating inflammatory and chronic neuropathic pain. Neurobiol. Pain 15, 100151; doi:10.1016/j.ynpai.2024.100151 (2024)..

[38] Joensuu, H., Ejlertsen, B., Lønning, P. E. & Rutqvist, L.-E. Aromatase inhibitors in the treatment of early and advanced breast cancer. Acta Oncol. 44, 23–31; doi:10.1080/02841860510007468 (2005).

[39] Myers, M., Britt, K. L., Wreford, N. G. M., Ebling, F. J. P. & Kerr, J. B. Methods for quantifying follicular numbers within the mouse ovary. Reproduction 127, 569–580; doi:10.1530/rep.1.00095 (2004).

[40] Can, A. et al. The mouse forced swim test. J. Vis. Exp. 59, e3638; doi:10.3791/3638 (2012).

Conflict of interest statement

The authors have no conflicts of interest to declare.

Acknowledgments

This study was supported by funding from the Korea Institute of Oriental Medicine (Project No. KSN2511011), National Research Foundation of Korea(NRF) grant funded by the Korea government(MSIT) (RS-2026-25587557) and Chungnam National University. All animal experiments were approved by the Institutional Animal Care and Use Committee of Chungnam National University (approval Nos. 202501A-CNU-007, 202512A-CNU-270).

All authors contributed to the study design, data acquisition, analysis, and interpretation of data, and approved the final manuscript.

The data generated in this study are included in this article. All data are available from the corresponding author upon reasonable request.

Figure legends

Figure 1. Schematic illustration of the experimental procedures and hormone depletion periods used to establish the ovariectomy (OVX), intraperitoneal injection of 4-vinylcyclohexene diepoxide (IP-VCD), and intraovarian injection of 4-vinylcyclohexene diepoxide (IO-VCD) models. The schematic illustration was generated using Biorender (BioRender.com).

Figure 2. Comparison of physiological and endocrine changes following hormone depletion in OVX, IP-VCD, and IO-VCD mice. (a,b,c) Body weight was measured at 5-day intervals for up to 80 days. Total body weight gain was analyzed at 30 days in the OVX and IO-VCD groups and at 80 days in the IP-VCD group, based on the onset of persistent estrous arrest in each model. Body weight gain among the three models was also compared at day 80. (Control, n = 5; each hormone depletion group, n = 7; unpaired two-tailed Student's t-test; $^{**}P < 0.01$, $^{***}P < 0.001$, $^{+}P < 0.05$, $^{++}P < 0.01$, $^{+++}P < 0.001$) (d-g) Representative uterine images and quantitative analysis of uterine weight and uterine diameter. Uterine diameter was measured between the two ends of the endometrium. (Scale bar: D = 1 cm; E = 200 μm; n = 5; one-way ANOVA followed by Bonferroni's post hoc test; $^{*}P < 0.05$, $^{***}P < 0.001$, $^{+}P < 0.05$, $^{+++}P < 0.001$, $^{\#}P < 0.05$, $^{\#\#\#}P < 0.001$) (h,i) Serum estradiol and androstenedione concentrations measured by ELISA. (Control, n = 5; each hormone depletion group, n = 7; one-way ANOVA followed by Bonferroni's post hoc test; $^{*}P < 0.05$, $^{**}P < 0.01$, $^{***}P < 0.001$) OVX, ovariectomy; IP-VCD, intraperitoneal injection of 4-vinylcyclohexene diepoxide; IO-VCD, intraovarian injection of 4-vinylcyclohexene diepoxide; ELISA: enzyme-linked immunosorbent assay.

Figure 3. Histological analysis of follicular depletion following VCD administration. (a) Representative

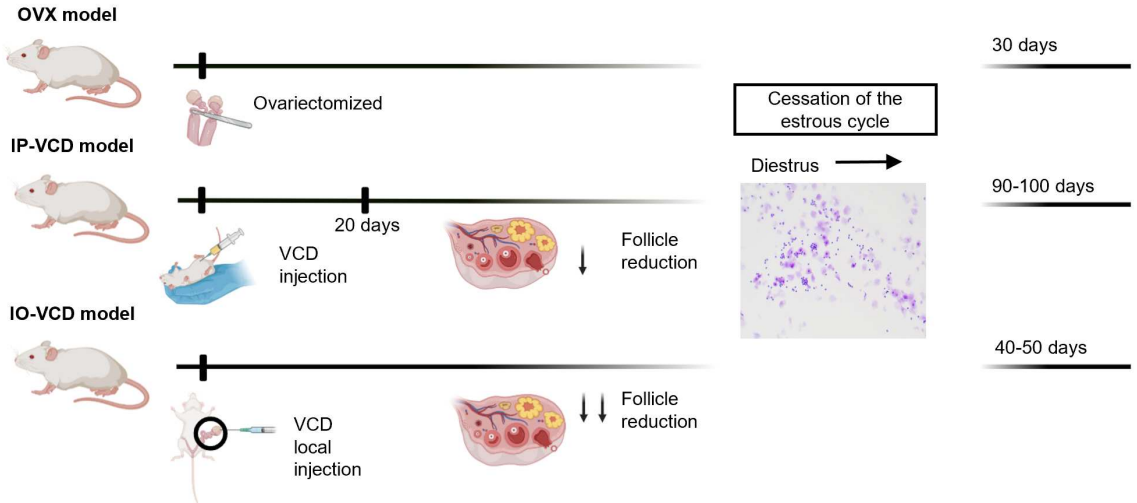
H&E-stained ovarian sections from the IP-VCD and IO-VCD models at the time of persistent estrous arrest. (b-d) Quantification of the numbers of primary, secondary, and antral follicles. (Scale bar = 200 μm; n = 5; unpaired two-tailed Student's t-test; $^{**}P < 0.01$, $^{***}P < 0.001$) OVX, ovariectomy; IP-VCD, intraperitoneal injection of 4-vinylcyclohexene diepoxide; IO-VCD, intraovarian injection of 4-vinylcyclohexene diepoxide.

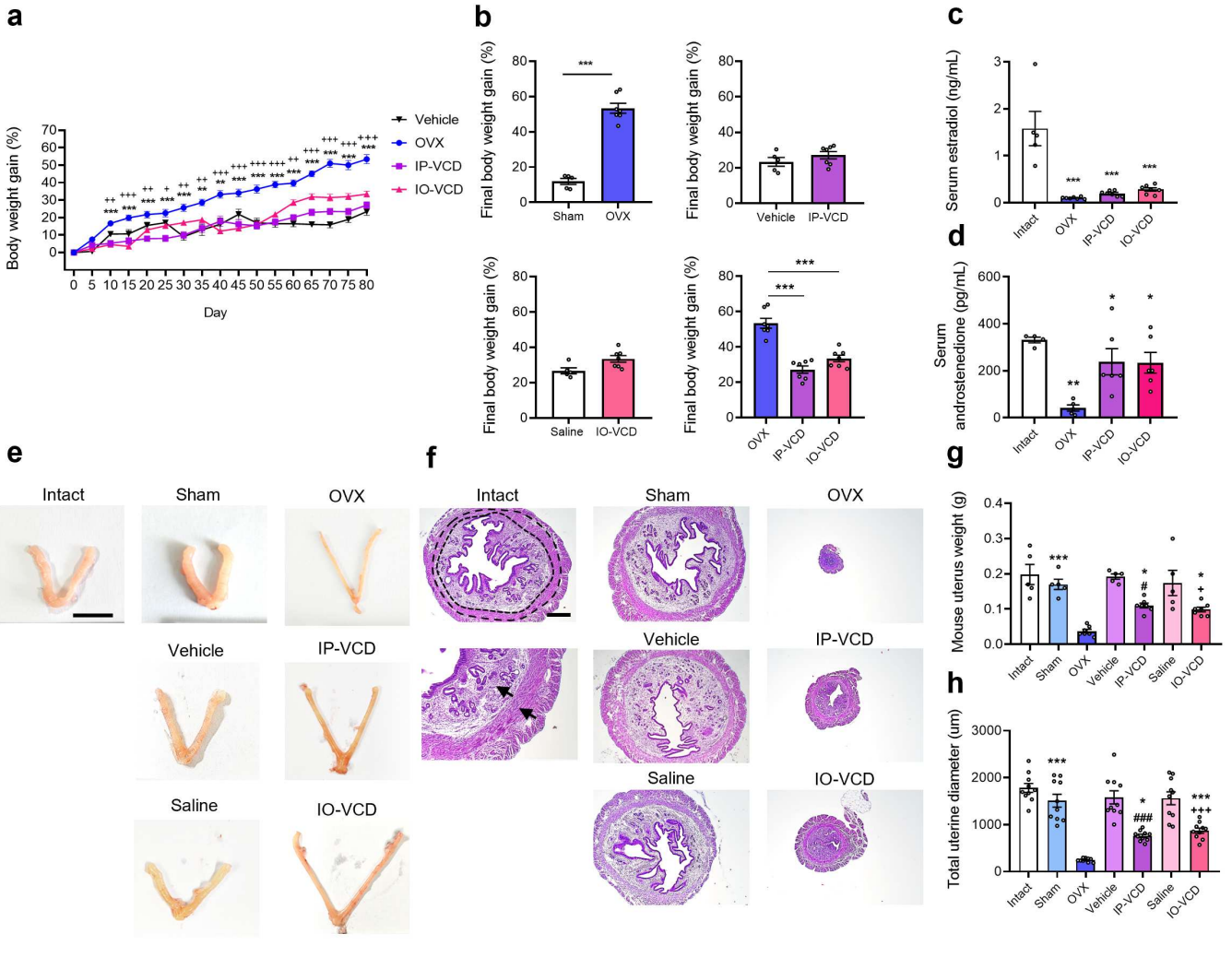
Figure 4. Effects of different hormone depletion models on exploratory activity and depression-like behavior. (a) Schematic illustration of the behavioral tests used to evaluate exploratory activity and depression-like behavior. (b–e) Representative movement traces recorded during the open field test (b) and quantification of time spent in the center zone (c), number of entries into the center zone (d), and total distance traveled (e). (n = 5–7; one-way ANOVA followed by Bonferroni's post hoc test) (f) Quantification of immobility time during the forced swim test. (n = 7–10; one-way ANOVA followed by Bonferroni's post hoc test; $^{*}P < 0.05$, $^{**}P < 0.01$) OVX, ovariectomy; IP-VCD, intraperitoneal injection of 4-vinylcyclohexene diepoxide; IO-VCD, intraovarian injection of 4-vinylcyclohexene diepoxide.

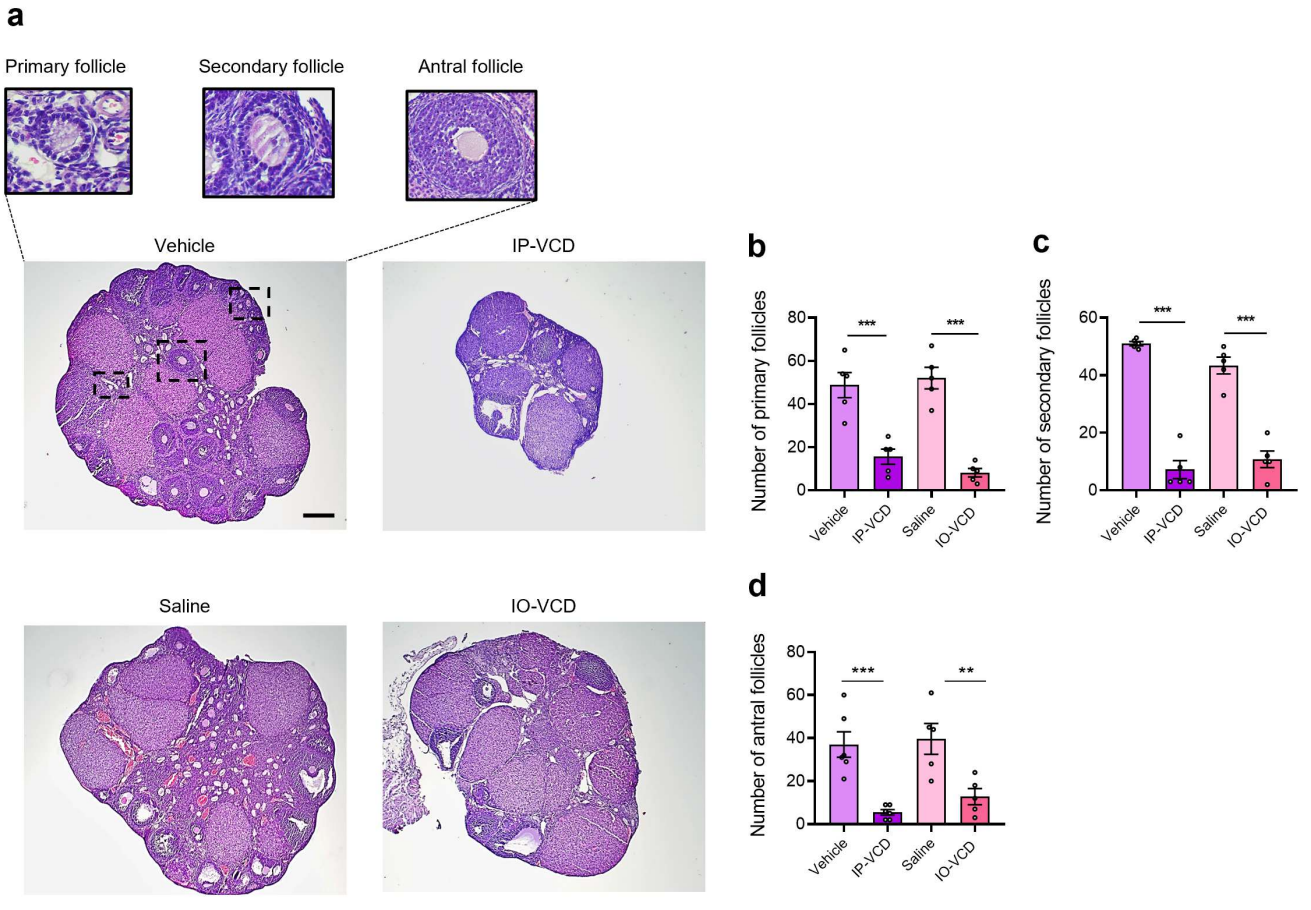
Figure 5. Effects of different hormone depletion models on formalin-induced pain behavior and spinal neuronal activation. (a-c) Pain behavior was analyzed during the first phase (0–15 min) and second phase (15–60 min) following formalin injection (a). Quantification of formalin-induced licking time during the first phase (b) and second phase (c). (n = 5–10; one-way ANOVA followed by Bonferroni's post hoc test; $^{*}P < 0.05$, $^{**}P < 0.01$) (d,e) Representative images of c-Fos immunofluorescence in the L4–L6 spinal dorsal horn following formalin injection (d) and quantification of c-Fos-positive neurons in laminae I–II of the spinal dorsal horn (e). (Scale bar = 100 μm; n = 5–10; one-way ANOVA followed by Bonferroni's post hoc test; $^{*}P < 0.05$, $^{**}P < 0.01$, $^{***}P < 0.001$) OVX, ovariectomy; IP-VCD, intraperitoneal injection of 4-vinylcyclohexene diepoxide; IO-VCD, intraovarian injection of 4-vinylcyclohexene diepoxide

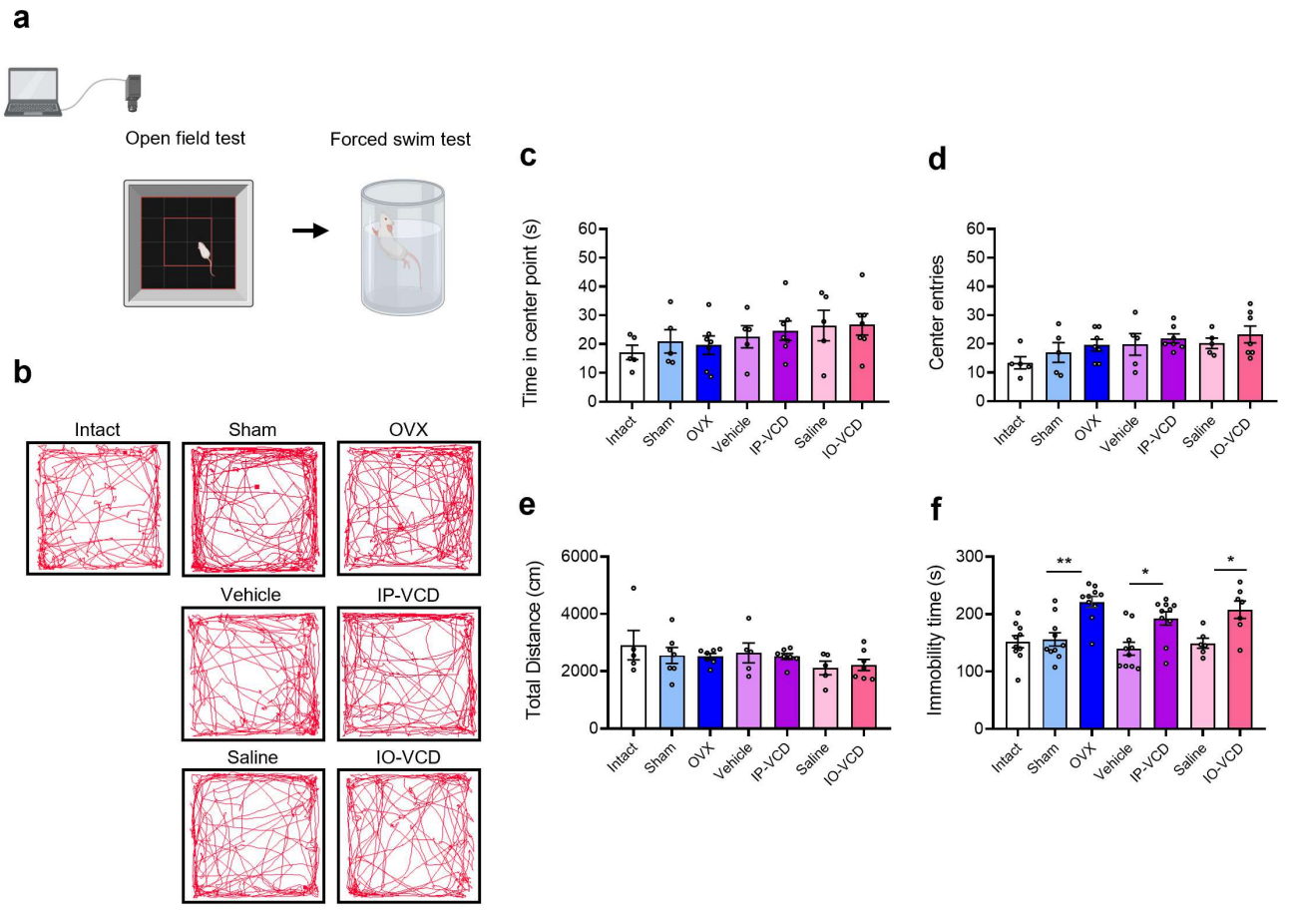
Figure 6. Changes in aromatase expression in the dorsal root ganglion (DRG) following hormone depletion induced by different methods. (a,b) Representative immunofluorescence images showing aromatase (green) expression and its cellular localization in the DRG by double immunofluorescence staining with glutamine synthetase (GS; red) and neuronal nuclei (NeuN; red). (Scale bar = 100 μm) (c-f) Quantification of aromatase immunofluorescence intensity according to neuronal size. DRG neurons were classified as small- (< 25 μm), medium- (25–35 μm), and large-diameter (> 35 μm) neurons. (n = 5; one-way ANOVA followed by Bonferroni's post hoc test; *P < 0.05, **P < 0.01, ***P < 0.001, +P < 0.05, ++P < 0.01, #P < 0.05, ##P < 0.01) OVX, ovariectomy; IP-VCD, intraperitoneal injection of 4-vinylcyclohexene diepoxide; IO-VCD, intraovarian injection of 4-vinylcyclohexene diepoxide.

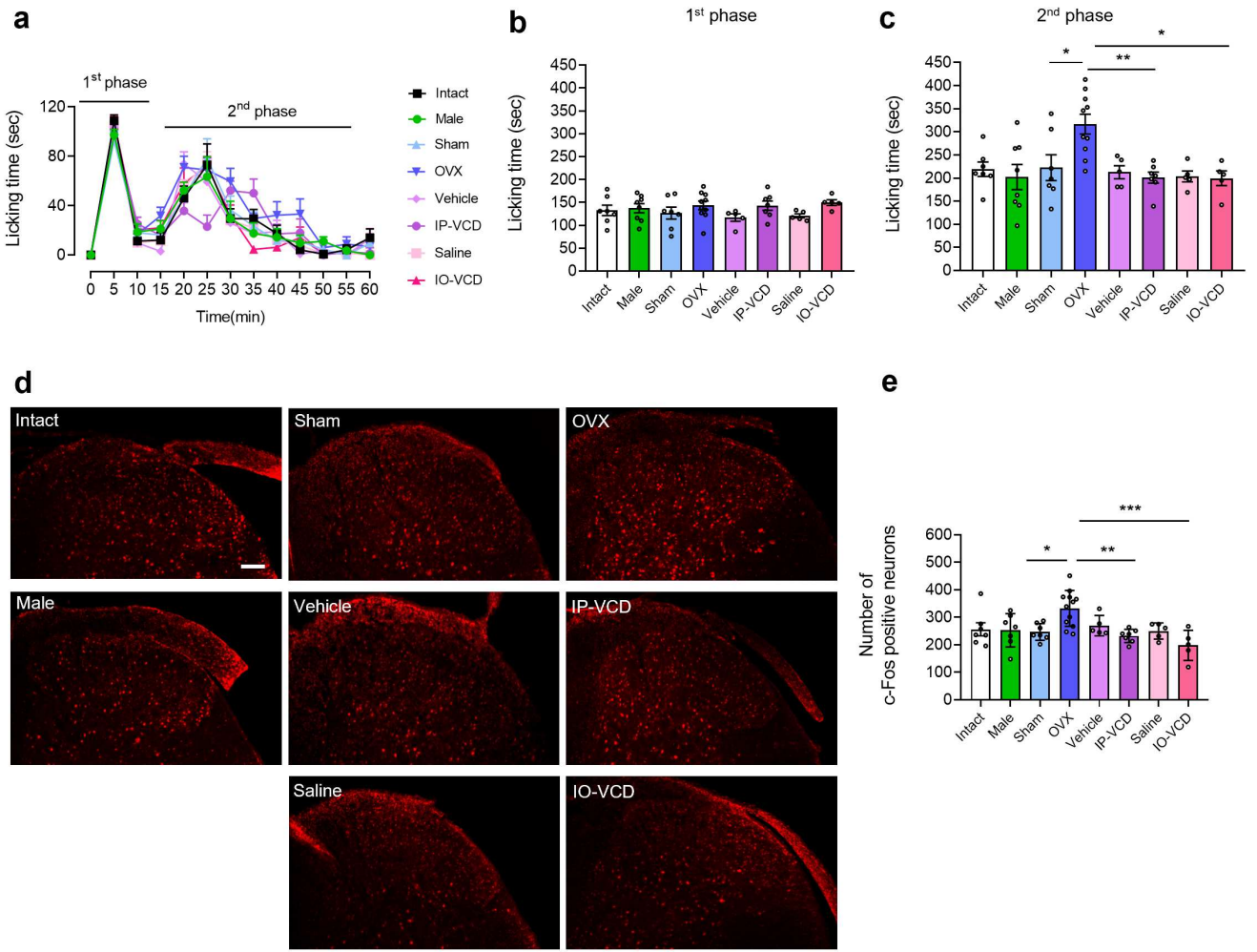
Figure 7. Effects of letrozole on formalin-induced pain behavior and spinal neuronal activation in the IP-VCD and IO-VCD models. (a–c) Pain behavior was analyzed during the first phase (0–15 min) and second phase (15–60 min) following formalin injection (a). Quantification of formalin-induced licking time during the first phase (b) and second phase (c). (n = 5; one-way ANOVA followed by Bonferroni's post hoc test; *P < 0.05, **P < 0.01) (D, E) Representative images of c-Fos immunofluorescence in the L4–L6 spinal dorsal horn following formalin injection in the letrozole-treated group (d) and quantification of c-Fos-positive neurons in laminae I–II of the spinal dorsal horn (e). (Scale bar = 100 μm; n = 5; one-way ANOVA followed by Bonferroni's post hoc test; **P < 0.01) OVX, ovariectomy; IP-VCD, intraperitoneal injection of 4-vinylcyclohexene diepoxide; IO-VCD, intraovarian injection of 4-vinylcyclohexene diepoxide.

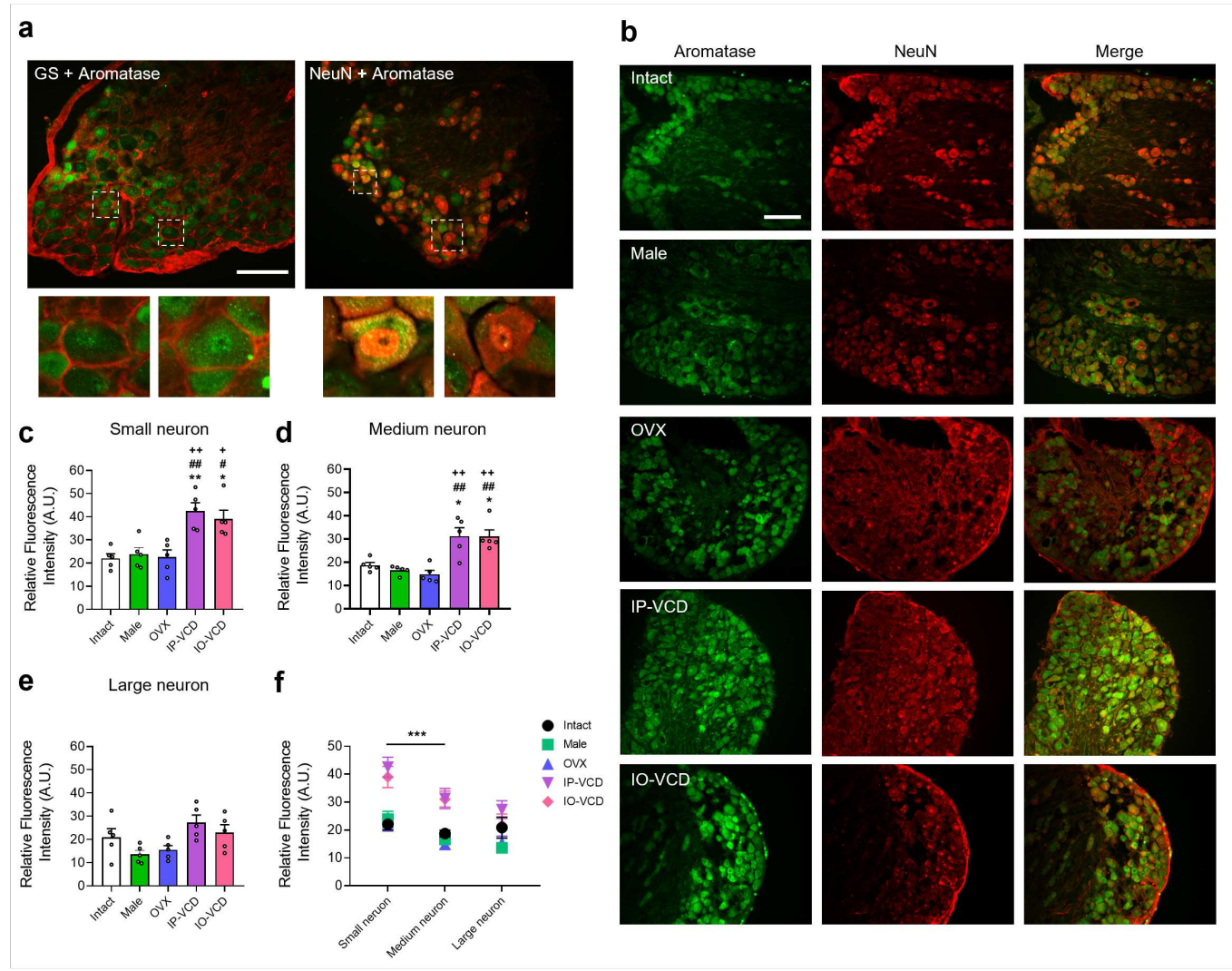

OVX model
Ovariectomized
30 days
Cessation of the estrous cycle
IP-VCD model
20 days
VCD injection
Follicle reduction
Diestrus
90-100 days
IO-VCD model
VCD local injection
Follicle reduction
40-50 days

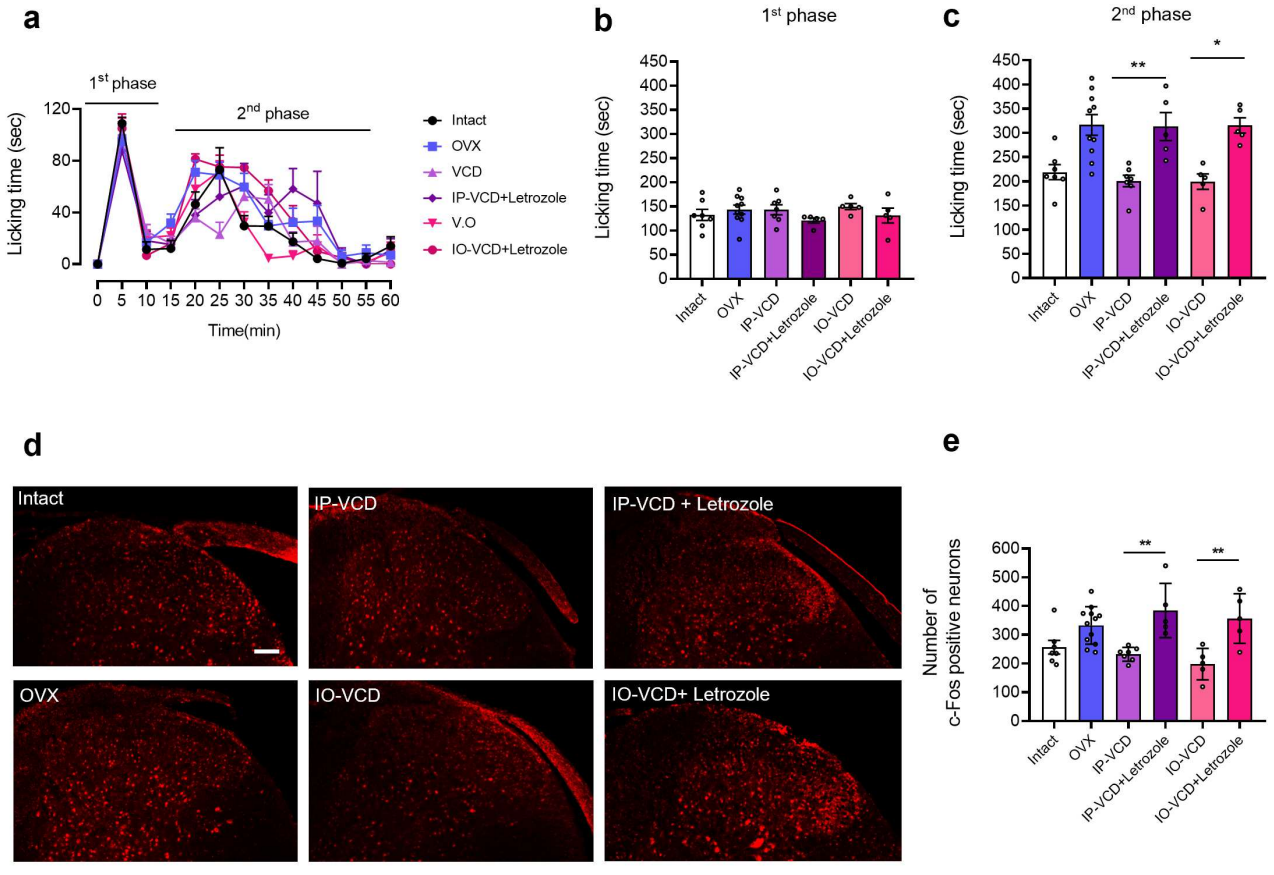

a
Body weight gain (%)
Day
Vehicle
OVX
IP-VCD
IO-VCD
b
Final body weight gain (%)
Sham
OVX
Vehicle
IP-VCD
Saline
IO-VCD
c
Serum estradiol (ng/mL)
Intact
OVX
IP-VCD
IO-VCD
d
Serum androstenedione (pg/mL)
e
Intact
Sham
OVX
Vehicle
IP-VCD
Saline
IO-VCD
f
g
Mouse uterus weight (g)
h
Total uterine diameter (um)


a
Primary follicle
Secondary follicle
Antral follicle
Vehicle
IP-VCD
Saline
IO-VCD
b
Number of primary follicles
***
***
Vehicle
IP-VCD
Saline
IO-VCD
c
Number of secondary follicles
***
***
Vehicle
IP-VCD
Saline
IO-VCD
d
Number of antral follicles
***
**
Vehicle
IP-VCD
Saline
IO-VCD


a
Open field test
Forced swim test
b
Intact
Sham
OVX
Vehicle
IP-VCD
Saline
IO-VCD
c
Time in center point (s)
d
Center entries
e
Total Distance (cm)
f
Immobility time (s)
**
*
*


a
1st phase
2nd phase
Licking time (sec)
Time(min)
Intact
Male
Sham
OVX
Vehicle
IP-VCD
Saline
IO-VCD
b
1st phase
Licking time (sec)
c
2nd phase
Licking time (sec)
d
Intact
Sham
OVX
Male
Vehicle
IP-VCD
Saline
IO-VCD
e
Number of
c-Fos positive neurons


a
GS + Aromatase
NeuN + Aromatase
b
Aromatase
NeuN
Merge
Intact
Male
OVX
IP-VCD
IO-VCD
c
Small neuron
Relative Fluorescence Intensity (A.U.)
Intact
Male
OVX
IP-VCD
IO-VCD
d
Medium neuron
e
Large neuron
f
***
Small neruon
Medium neuron
Large neuron


a
1st phase
2nd phase
Licking time (sec)
120
80
40
0
0 5 10 15 20 25 30 35 40 45 50 55 60
Time(min)
Intact
OVX
VCD
IP-VCD+Letrozole
V.O
IO-VCD+Letrozole
b
1st phase
Licking time (sec)
450
400
350
300
250
200
150
100
50
0
Intact
OVX
IP-VCD
IP-VCD+Letrozole
IO-VCD
IO-VCD+Letrozole
c
2nd phase
Licking time (sec)
**
*
d
Intact
IP-VCD
IP-VCD + Letrozole
OVX
IO-VCD
IO-VCD+ Letrozole
e
Number of c-Fos positive neurons
600
500
400
300
200
100
0
**
**